University of Glasgow

DEPARTMENT OF

AEROSPACE ENGINEERING

Individual Blade Rotor Model for Use in Inverse Simulation

Stephen Rutherford, Dr. Douglas G. Thomson

Internal Report No. 9604

May 1996

Individual Blade Rotor Model for Use in Inverse Simulation

Stephen Rutherford, Dr. Douglas G. Thomson

Internal Report No. 9604
May 1996

Summary

The individual blade rotor model, "*Hibrom*" has been developed for use in inverse simulation of a helicopter. This report details the modelling assumptions made and the equations required to calculate the forces and moments produced by the main rotor.

Contents

1 Introduction

To successfully simulate the dynamics of a given aircraft requires calculation of the forces and moments generated by each of the vehicle's components. For a helicopter, modelling the main rotor occupies the majority of effort as this is the most complex component and produces the greatest forces and moments. The forces and moments generated by a helicopter rotor are most conveniently estimated by use of Blade Element Theory. In the context of helicopter simulation there are two commonly adopted approaches : the "Disc Model" and the "Individual Blade Model". Disc type models[1] represent the main rotor by a single uniform annulus which is assumed steady for any given flight state, and has a solidity determined by the number of blades and their geometry. Using simplifying assumptions, such as linear aerodynamic properties, expressions can be developed for the elemental forces which, when integrated analytically over the whole disc, yield estimates of the forces and moments acting at the main rotor hub centre. By contrast, individual blade models[2,3], of which "Hibrom" is an example, represent each blade separately. Numerical integration of the forces acting upon a discrete element allows fewer modelling simplifications to be made and hence more accurate determination of the forces and moments acting at each blade hinge. In addition treatment of each blade individually facilitates observation of their respective dynamics. In both cases correct modelling of the rotor additionally requires blade element modelling to be combined with either Vortex or Momentum Theory. In Vortex Theory[4] the flow of the air over a blade is considered in 3-dimensions and the downwash distribution related to the magnitude and distribution of the wake structure. To accurately model a rotating, manoeuvring rotor system in this way, however, is computationally intensive and outwith the scope of this work. Consequently the forces and moments produced by the main rotor are determined by Blade Element / Momentum Theory[4] where the thrust produced by the whole rotor is related to the downwash (or inflow velocity) distribution over the plane of the disc. The dynamic inflow model used in Hibrom is that of Peters and HaQuang[5].

Determination of the rotor forces and moments is detailed in Section 3, but first the main modelling features and simplifying assumptions will be discussed.

2. Modelling Assumptions

As, to the best of the author's knowledge, no previous attempts have been made to incorporate an individual blade model in inverse simulation, it was decided to restrict the number of modelling features to a manageable level. This should avoid clouding the issue of implementing the model in an inverse simulation framework. Clearly this does not rule out model augmentation at a later date. The modelling assumptions are as follows.

Ideal atmospheric conditions.

Calm International Standard Atmosphere conditions are assumed. No attempt has been made to model the influence of either gusts or a steady wind. As most results will concern Nap-of-the-Earth flight, the air density is that at sea level. Future rate of climb and hover ceiling tests will, however, consider the change in air density. Typical manoeuvres will be low altitude though of sufficiently high speed to neglect Ground Effect.

2D aerodynamics.

As trailing vortices are not modelled, the spanwise flow over the blade is not considered. Consequently the aerodynamic forces are accepted to consist of components only parallel and perpendicular to the aerofoil angle of attack. These forces are assumed to act through the aerodynamic centre, understood to be coincident with the quarter chord point. The aerodynamic pitching moment about this point is ignored implying torsional rigidity.

Dynamic inflow model.

The behaviour of the flow around a helicopter rotor is, in reality, very complex. However attempts have previously been made to model this flow using Vortex Theory, culminating in either a prescribed or free wake model. Though a prescribed wake model has been used successfully with wind turbines it is of no use in the manoeuvring flight of inverse simulation. A free wake model was precluded due to its computational intensity and the development time required. Thus to simulate the wake was deemed impractical. Having abandoned vortex theory the obvious alternative is Blade Element / Momentum theory where the flow over the aerofoil and the induced velocity are treated separately using 2D aerodynamics and the Peters-HaQuang dynamic inflow model respectively. The nature of vortices and hence blade-vortex interactions in the wake are not examined.

It is necessary to observe the velocity induced on the local airstream by a rotating system of blades as this has an effect on the resultant velocity, the local angle of attack and consequently the aerodynamic forces generated by the rotor. A commonly used, rudimentary model for estimating the inflow velocity is based upon momentum theory as developed by Glauert[4]. In Glauert's model the inflow consists of a uniform velocity component which is related to the thrust generated by the rotor. To this is superimposed azimuthally and radially varying harmonic components, the magnitude of which are determined by the flight state. Thus the inflow distribution, as a function of radial and azimuthal position, can be calculated for the entire rotor plane. There are, however, two main problems with this formulation ; namely that the air is assumed to accelerate instantaneously as it crosses the plane of the disc, and that the effects of pitching and rolling moments are disregarded. More sophisticated inflow models attempt to address these limitations. Firstly, as determination of the inflow velocities is governed by a first order differential equation, the lag between the application of pitch changes and thrust changes is modelled. The effects of the pitching and rolling moments are also observed, and the inflow velocities and accelerations are related by a gains matrix. The rotor model discussed here uses the dynamic model of Peters and HaQuang (Section 5) which is a development of the earlier model of Pitt and Peters[6]. It is currently the only dynamic inflow model which takes into account the effect of sideward flight and thus the most suitable model for use in inverse simulation. In his review of inflow models Chen[7] states that "correlation with several sets of test data indicate that the Pitt/Peter's first harmonic inflow model works well", further reinforcing its suitability.

Inertial forces.

As the inertial (other than spanwise) forces acting upon the rotor are much smaller than the aerodynamic forces, they are omitted from some models. Derivation of the accelerations and subsequently inertial forces has, however, been included here.

Constant rotorspeed.

Due to computational problems discussed elsewhere[8], the discretisation interval used in inverse simulation has to match one complete period of the rotor (1 / 4 revolution for a 4 bladed rotor in Hibrom). For initial manageability in inverse simulation a constant rotorspeed is assumed, thus allowing the discretisation interval to be predicted early in the computational process. A variable rotorspeed would require a variable discretisation size which in manoeuvring flight would be extremely difficult to ascertain.

Blade Dynamics.

Blade Elasticity. The elastic deformation of the blades due to their loading has been deemed beyond the scope of this research. Turnour and Celi[9] suggest that elastic modelling "has a very small effect on the dynamics of the helicopter" for articulated rotors. This claim is reinforced by Lewis[10]. As Hibrom is predominantly to be used for flight dynamics, the assumption of fully rigid rotor blades would therefore appear to be reasonable. It is however anticipated that the off-axis vehicle response will not be as accurate when simulating semi-rigid rotors, Sturisky and Schrage[11]. Mansur[3], who uses a similar rigid individual blade model to simulate the AH-64A Apache, concurs that on-axis responses do match flight test data much better than off-axis. Hill, DuVal et al.[14] find that elastic models demonstrate improved correlation with flight test data, and as such should be considered for future development.

Lead / lag freedom. The periodicity of the coriolis effect and the drag force from the blades means that a helicopter rotor requires a lead / lag damper to alleviate fatigue damage. Lead / lag dynamics have not, however, been included in Hibrom. The implicit, balancing assumption is that the in-plane stiffness and strength of the hinge are sufficient to prevent motion without structural damage.

Torsional freedom. As already stated, elastic effects have been neglected i.e. torsional rigidity is assumed. Torsional freedom would also add undesireable complications due to the change in effective blade pitch.

Flap freedom. Though torsional and lead / lag dynamics have been neglected, flap displacements are of sufficent magnitude that to ignore them would result in very poor prediction of the rotor forces and moments. The full second order differential equations which govern the flapping dynamics of a blade have been included in the rotor model and their development from first principles is given in Section 4.

Aerodynamic Data.

Compressibility effects. For aerofoils travelling at subsonic speeds the effect of the high pressure region immediately in front of the leading edge can propogate upstream, thus 'preparing' the air for the influence of the aerofoil and ensuring smooth passage around it. At supersonic speeds, however, the influence of the high pressure region (transmitted at the speed of sound) is incapable of making its presence felt upstream and there exists a shock wave (discontinuity) between the subsonic flow at the leading edge of the aerofoil and the supersonic flow in the freestream. Consequently the characteristics of

subsonic and supersonic flow are very different. In transonic flow there may exist local areas of supersonic flow such as on the upper surface of the aerofoil. Thus as Mach number increases, even at subsonic speeds, the lift and drag on the aerofoil can change. This is reflected in the empirically derived aerodynamic look-up tables which are functions of both local angle of attack and Mach number. As the Mach number increases for a given angle of attack, and the aerofoil moves from the subsonic to transonic region, the lift coefficient decreases and the drag coefficient increases. Hence the effect of air compressibility local to a blade element is considered.

Angle of attack range. The individual blade model documented here is intended to be used in inverse simulation of compound helicopter configurations whose rotors' aerodynamic limits are unknown. Disc models are limited to simulating helicopters with established control limits, as assuming the linear relationship, $C_L = a_0\alpha$ does not acknowledge blade stall and can allow solutions at unrealistically high blade pitch angles. Individual blade models can also suffer from this shortcoming if aerodynamic data is not available for a wide range of angles of attack, α. Rather than limit the angle to which the inverse simulation algorithm can pitch the blades - thus implying the control limits are known - it was considered desirable to extend the angle of attack data into the fully stalled region and thus simulate control failure at too high a speed or for too severe a manoeuvre. In addition, the high speed flight of compound helicopters may result in a large reversed flow region on the retreating side of the rotor. In such a region the effect is that of air passing over an aerofoil section from trailing edge to leading edge. As the blade sections in question are both reversing and invariably at a negative local angle of attack they produce negative lift; relatively high drag; and have rapid, abrupt stall characteristics. The inclusion of aerodynamic data for the full 360° angle of attack range also allows this phenomenon of reversed flow to be modelled. As post stall aerodynamic forces are caused predominantly by bluff body effects, compressibility has been neglected for the data at high angles of attack. It is also reasonable to ignore compressibility effects in the reversed flow region as the local air encountered will always be at low speed. All empirically obtained aerodynamic data is for an aerofoil immersed in steady flow, thus the effect of dynamic stall is not included.

High angle of attack and reversed flow aerodynamic data is particularly useful for observing the behaviour of retreating blades which, in tandem with the compressibility effects - significant for the advancing blade - enhances modelling of high speed flight.

Effective hinge offset.

From the earlier statement that the blades are fully rigid it can be assumed that all

blade flapping occurs as a result of angular displacements about an idealised hinge. The hinge has to be modelled in such a fashion as to give a reasonable estimate of the forces and moments acting at the rotor hub centre. Any semi-rigid or fully-articulated rotor can thus be modelled in one of three ways : by a centrally sprung hinge with a restoring moment related to the flapping angle by the equivalent spring stiffness; a free pivot with no restoring moment but positioned some distance - the effective hinge offset - from the hub centre; or a combination of spring stiffness and hinge offset[12]. The hinge model chosen here is the effective hinge offset with no spring stiffness, where the value for the effective hinge offset achieves the correct flapping frequency based upon assumptions made by Padfield[13]. A semi-rigid rotor is represented by a large hinge offset ; a fully-articulated rotor by a relatively small value.

Blade geometry.

Blade Twist. In a rotating system the tip of each blade has a much higher local velocity than the root i.e. the local velocity is directly related to the radial position. As the aerodynamic forces are proportional to the velocity squared then clearly much more lift can be generated in the outboard section of the blade. To produce a more uniform lift distribution and reduce the bending moment at the hinge, blades are manufactured with a spanwise geometric twist where the pitch at the tip is reduced relative to that at the root - typically in the region of 6-10°. A linear twist variation has been included in the elemental data.

Chord variation. Disc type models commonly assume a constant chord in order to simplify algebraic expressions. In practice, however, helicopter blades posess a variable chord due to, for example, the root cut out or swept back tips. To vary the dimensions of the chord in individual blade models is a trivial problem and accordingly chord variation has been incorporated simply by using discrete values for each element.

The individual blade model will now be detailed.

3. Individual Blade Model for Helicopter Main Rotor

The familiar Euler rigid body equations (Appendix 1) form the basis of simulating the motion of the helicopter fuselage. They are expressed in terms of the body velocities and accelerations (U, V, W, P, Q, R and their derivatives) and the external forces and moments (X, Y, Z, L, M, N) which include components from the main rotor. As the rotor model is an individual blade type and is based upon blade element theory, it follows that its contribution to the external forces and moments requires knowledge of the velocity and acceleration, referred to local axes, of each blade element. In formulating such expressions it is initially assumed that the elements are of unit span, that the velocities and accelerations are uniform over each element and are equal to those at the elemental centres. Thus starting from known body velocities and accelerations, determination of the desired values involves a series of axes transformations, culminating in the velocity and acceleration of a blade element referred to the local blade axis set. Figure 1 shows the axis sets relating an individual blade element to the helicopter centre of gravity. The development of the velocity and acceleration of a blade element is now detailed.

3.1 Kinematics of a Blade Element

3.1.1 Velocity of a Blade Element

For a rigid system, the general expression for the absolute velocity of a point, p, referred to an orthogonal axis set q, fixed in relation to origin o, is given as :

$$\underline{v}_p^q = \underline{v}_o^q + \frac{d\underline{r}_{o/p}^q}{dt} = \underline{v}_o^q + \underline{\omega}^q \times \underline{r}_{o/p}^q, \qquad (1)$$

where $\underline{v}_o^q$ is the linear velocity of the origin, o, of the axis set q;

$\underline{r}_{o/p}^q$ is the vector describing the position of point p relative to origin o, referred to the axis set q; and

$\underline{\omega}^q$ is the rotational velocity of the axis set, q, about the origin of the axes, o.

Now considering the specific case of the modelled rotor system, the first stage is to describe, in *body* axes, the velocity of the hub centre with respect to the helicopter's centre of gravity. Thus from equation (1) the hub velocity can be expressed as :

Figure 1 : Axis Sets Relating Rotor Blade Elemental Position to Helicopter Centre of Gravity

$$\underline{v}_{hub}^{body} = \underline{v}_{c.g.}^{body} + \underline{\omega}^{body} \times \underline{r}_{c.g./hub}^{body},$$

where

$$\underline{v}_{c.g.}^{body} = \{U \quad V \quad W\}^{\mathrm{T}},$$

$$\underline{\omega}^{body} = \{P \quad Q \quad R\}^{\mathrm{T}},$$

$$\underline{r}_{c.g./hub}^{body} = \{x_{ref.} + l_{hub} \quad 0 \quad z_{ref.} + h_{hub}\}^{\mathrm{T}},$$

and $x_{ref.}$, $z_{ref.}$ are distances along the $\underline{i}^{body}$ and $\underline{k}^{body}$ axes from the helicopter centre of gravity to the fuselage reference point (the fuselage reference point is both the point at which the fuselage's aerodynamic loadings are referred and the datum from which all other points on the helicopter are measured) ;

and l_{hub}, h_{hub} are distances along the $\underline{i}^{body}$ and $\underline{k}^{body}$ axes from the fuselage reference point to the hub centre i.e. the hub height above and length fore / aft of the fuselage reference point.

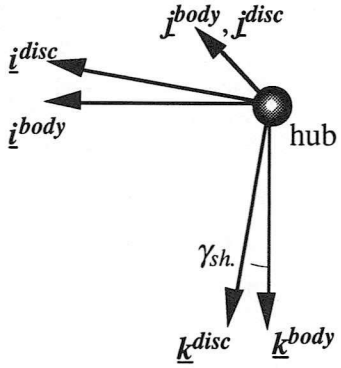

Figure 2 : Transformation from Body to Disc Axis Set

It is assumed that the rotor shaft is inclined with respect to the body axes by the shaft tilt angle, $\gamma_{sh.}$ and hence the hub velocity must be related to an axis set aligned with the shaft. Referring to Figure 2, the linear and rotational hub velocities should be expressed in terms of the *disc* axis set, centred at the hub and fixed in relation to the body axes set. This is achieved by rotation about the $\underline{j}^{body}$ axis through the shaft tilt angle :

$$\begin{aligned} \underline{v}_{hub}^{disc} &= \left[T^{body/disc}\right] \underline{v}_{hub}^{body} \\ &= \{u_{hub}^{disc} \quad v_{hub}^{disc} \quad w_{hub}^{disc}\}^{\mathrm{T}}, \\ \underline{\omega}^{disc} &= \left[T^{body/disc}\right] \underline{\omega}^{body}, \end{aligned} \tag{2}$$

where the transformation matrix from body to disc axes is given as :

$$\left[T^{body/disc}\right]=\begin{bmatrix}\cos\gamma_{sh.} & 0 & -\sin\gamma_{sh.}\\ 0 & 1 & 0\\ \sin\gamma_{sh.} & 0 & \cos\gamma_{sh.}\end{bmatrix}. \tag{3}$$

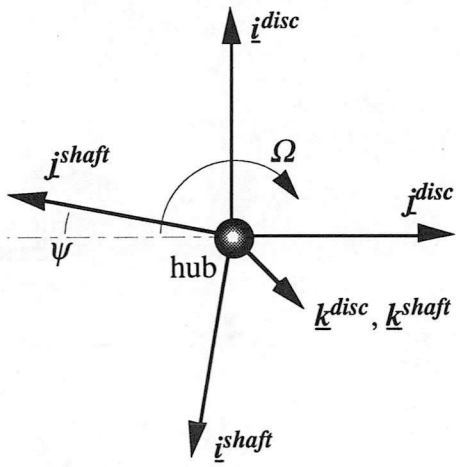

Figure 3 : Transformation from Disc to Shaft Axis Set

The next step is to refer the hub velocities to the *shaft* axis set, Figure 3. Like the disc axis set, the shaft axes are centred at the hub. Unlike the disc axes, though, the shaft set is a rotating one. For the linear velocity the transformation simply involves rotation about the $\underline{k}^{disc}$ axis through the shaft azimuth angle ψ, however, the rotational velocity must also include the rotorspeed, $\Omega = \dot{\psi}$. Thus :

$$\underline{v}_{hub}^{shaft} = \left[T^{disc/shaft}\right]\underline{v}_{hub}^{disc},$$

$$\begin{aligned}\underline{\omega}^{shaft} &= \left[T^{disc/shaft}\right]\underline{\omega}^{disc} + n_{clock}\left\{0 \quad 0 \quad \Omega\right\}^{\mathrm{T}}\\ &= \left\{p^{shaft} \quad q^{shaft} \quad r^{shaft}\right\}^{\mathrm{T}}\end{aligned} \tag{4}$$

where the integer n_{clock} ensures consistency with a right handed axis set i.e. a clockwise rotating rotor when viewed from above has $n_{clock} = 1$ and an anticlockwise rotating rotor has $n_{clock} = -1$. The disc to shaft transformation matrix is given as :

$$\left[T^{disc/shaft}\right]=\begin{bmatrix}-\cos\psi & -\sin\psi & 0\\ \sin\psi & -\cos\psi & 0\\ 0 & 0 & 1\end{bmatrix}. \tag{5}$$

If the helicopter is modelled with no hinge offset then the linear velocity of the hinge is equal to that of the hub centre; otherwise the contribution due to the effective hinge offset must be included. Hence :

$$\underline{v}_{hinge}^{shaft} = \underline{v}_{hub}^{shaft} + \underline{\omega}^{shaft} \times \underline{r}_{hub/hinge}^{shaft},$$

where $$\underline{r}_{hub/hinge}^{shaft} = \left\{ x_{hinge} \quad 0 \quad 0 \right\}^{\mathrm{T}}.$$

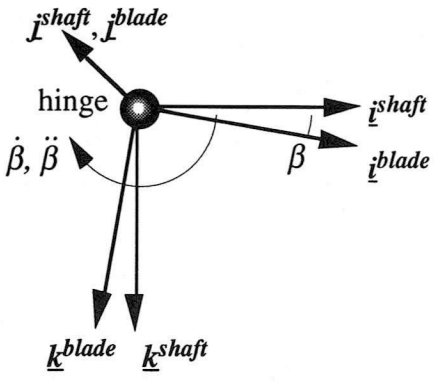

Figure 4 : Transformation from Shaft to Blade Axis Set

The linear velocity of the hinge expressed in *blade* axes is now calculated by rotation of blade flap angle, β about the $\underline{j}^{shaft}$ axis. Figure 4 illustrates the transformation from the shaft to the rotating blade axes set. The rotational velocity of the blade axes set, of which the hinge is the origin, is similarly transformed and the flapping rate, $\dot{\beta}$, then added to the $\underline{j}^{blade}$ component.

$$\underline{v}_{hinge}^{blade} = \left[T^{shaft/blade} \right] \underline{v}_{hinge}^{shaft},$$

$$\underline{\omega}^{blade} = \left[T^{shaft/blade} \right] \underline{\omega}^{shaft} + \left\{ 0 \quad \dot{\beta} \quad 0 \right\}^{\mathrm{T}}. \tag{6}$$

Equation (7) describes the transformation from shaft to blade axes :

$$\left[T^{shaft/blade} \right] = \begin{bmatrix} \cos\beta & 0 & -\sin\beta \\ 0 & 1 & 0 \\ \sin\beta & 0 & \cos\beta \end{bmatrix}, \tag{7}$$

where the instantaneous values of β and $\dot{\beta}$ are determined by the blade flapping equations in Section 4. Finally the linear velocity of each element, referred to blade axes, can be calculated by considering the spanwise distance from the hinge offset to the

respective elemental centre, $\underline{r}^{blade}_{hinge/elem.}$:

$$\underline{v}^{blade}_{elem.} = \underline{v}^{blade}_{hinge} + \underline{\omega}^{blade} \times \underline{r}^{blade}_{hinge/elem.}$$
$$= \left[u^{blade}_{elem.} \quad v^{blade}_{elem.} \quad w^{blade}_{elem.} \right]^{\mathrm{T}}, \tag{8}$$

where $$\underline{r}^{blade}_{hinge/elem.} = \left\{ r_{elem.} \quad 0 \quad 0 \right\}^{\mathrm{T}}.$$

Having calculated the linear velocities it is possible to evaluate the aerodynamic forces acting upon each blade element, but first the local acceleration of each blade element is detailed.

3.1.2 Acceleration of a Blade Element

The acceleration of a blade element, referred to local axes, is needed to calculate the inertial forces acting on each blade, which when added to the aerodynamic forces yield the total forces acting upon the rotor hub. The spanwise inertial (centripital) force is of particular importance as it is needed to balance the aerodynamic forces in the flap plane (and also in the lag plane if the lag degree of freedom were modelled). By comparison the chordwise and perpendicular inertial forces are small but to ensure consistency are included here nonetheless. The formulation of the accelerations will now be described though, as the procedure is similar, less pedantically than for the velocities. As with the velocities let us first consider the general formulation for a rigid system, so that the absolute acceleration of a point, p, referred to an orthogonal axis set, q, fixed in relation to origin o can be expressed as :

$$\underline{a}^q_p = \underline{a}^q_o + \frac{d^2 \underline{r}^q_{o/p}}{dt} = \underline{a}^q_o + \underline{\omega}^q \times \left(\underline{\omega}^q \times \underline{r}^q_{o/p} \right) + \underline{\alpha}^q \times \underline{r}^q_{o/p}, \tag{9}$$

where $\underline{a}^q_o$ is the linear acceleration of the origin, o, of the axis set q;

and $\underline{\alpha}^q$ is the rotational acceleration of the axis set, q, about the origin of the axes, o;

and the other terms are as defined earlier.

It thus follows from equation (9) that the acceleration of the hub centre in body axes can be expressed as :

$$\underline{a}_{hub}^{body} = \underline{a}_{c.g.}^{body} + \underline{\omega}^{body} \times \left(\underline{\omega}^{body} \times \underline{r}_{c.g./hub}^{body} \right) + \underline{\alpha}^{body} \times \underline{r}_{c.g./hub}^{body},$$

where the linear and rotational accelerations of the centre of gravity, in body axes, are respectively :

$$\underline{a}_{c.g.}^{body} = \begin{Bmatrix} \dot{U} + WQ - VR \\ \dot{V} + UR - WP \\ \dot{W} + VP - UQ \end{Bmatrix},$$

$$\underline{\alpha}^{body} = \left\{ \dot{P} \quad \dot{Q} \quad \dot{R} \right\}^{T},$$

and $\underline{\omega}^{body}$ and $\underline{r}_{c.g./hub}^{body}$ are as before. The accelerations are next transformed to disc axes, then shaft axes, and the rate of change of the rotorspeed (if variable rotor speed is modelled) added to the $\underline{k}^{shaft}$ term of the rotational acceleration so that :

$$\underline{a}_{hub}^{disc} = \left[T^{body/disc} \right] \underline{a}_{hub}^{body},$$

$$\underline{\alpha}^{disc} = \left[T^{body/disc} \right] \underline{\alpha}^{body},$$

$$\underline{a}_{hub}^{shaft} = \left[T^{disc/shaft} \right] \underline{a}_{hub}^{disc},$$

and $$\underline{\alpha}^{shaft} = \left[T^{disc/shaft} \right] \underline{\alpha}^{disc} + n_{clock} \left\{ 0 \quad 0 \quad \dot{\Omega} \right\}^{T}.$$

Now it is possible to find the linear acceleration of the hinge expressed in shaft, and - via transformation through flap angle, β - blade axes :

$$\underline{a}_{hinge}^{shaft} = \underline{a}_{hub}^{shaft} + \underline{\omega}^{shaft} \times \left(\underline{\omega}^{shaft} \times \underline{r}_{hub/hinge}^{shaft} \right) + \underline{\alpha}^{shaft} \times \underline{r}_{hub/hinge}^{shaft},$$

$$\underline{a}_{hinge}^{blade} = \left[T^{shaft/blade} \right] \underline{a}_{hinge}^{shaft}. \tag{10}$$

Finally the linear acceleration of the centre of a blade element can be evaluated :

$$\underline{a}_{elem.}^{blade} = \underline{a}_{hinge}^{blade} + \underline{\omega}^{blade} \times \left(\underline{\omega}^{blade} \times \underline{r}_{hinge/elem.}^{blade} \right) + \underline{\alpha}^{blade} \times \underline{r}_{hinge/elem.}^{blade}, \tag{11}$$

where the rotational acceleration of the blade axes, $\underline{\alpha}^{blade}$, is determined by transformation from the shaft axis set and inclusion of the second order flap derivative, $\ddot{\beta}$ as derived in Section 4 :

$$\underline{\alpha}^{blade} = \left[T^{shaft/blade}\right]\underline{\alpha}^{shaft} + \left\{0 \quad \ddot{\beta} \quad 0\right\}^{T}, \tag{12}$$

allowing calculation of the inertial forces acting on each element.

3.2 Rotor Forces and Moments

3.2.1 Aerodynamic Forces Acting Upon a Blade Element

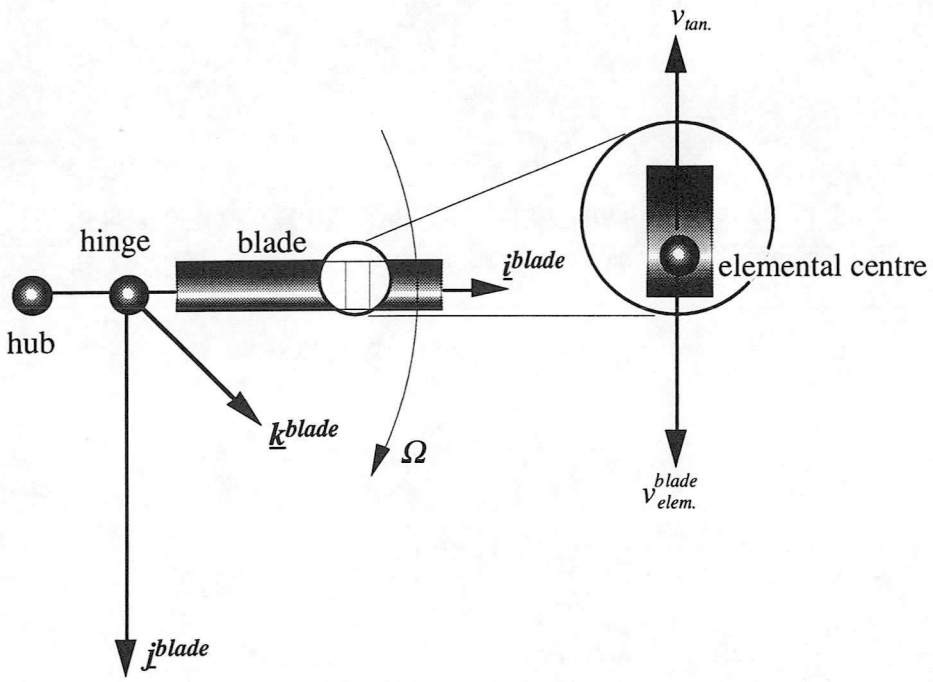

Figure 5 : Tangential Component of Velocity : Clockwise Rotating Rotor

The velocity of a blade element derived in Section 3.1.1 (equation 8) can be used to calculate the aerodynamic forces acting upon each element of unit span. Assuming two-dimensional aerodynamics then the lift and drag per unit span are $\bar{l}_{elem.}$ and $\bar{d}_{elem.}$ respectively. To calculate these forces it is first necessary to determine the tangential and perpendicular components of the velocity of the air over the blade i.e. in the opposite sense to the motion of the blade itself. Thus if the chordwise blade motion is in the same direction as the $\underline{j}^{blade}$ axis (as for a clockwise rotating rotor, Figure 5) then the tangential component of velocity is given by :

$$v_{tan.} = v_{elem.}^{blade}.$$

For an anticlockwise rotating rotor it is apparent that the chordwise velocity and

$\underline{j}^{blade}$ axis are in opposite directions, so the tangential velocity is defined as :

$$v_{tan.} = -v_{elem.}^{blade},$$

and using the integer flag n_{clock} defined earlier it is possible to define a single expression applicable to both clockwise and anticlockwise rotating systems :

$$v_{tan.} = n_{clock} v_{elem.}^{blade}.$$

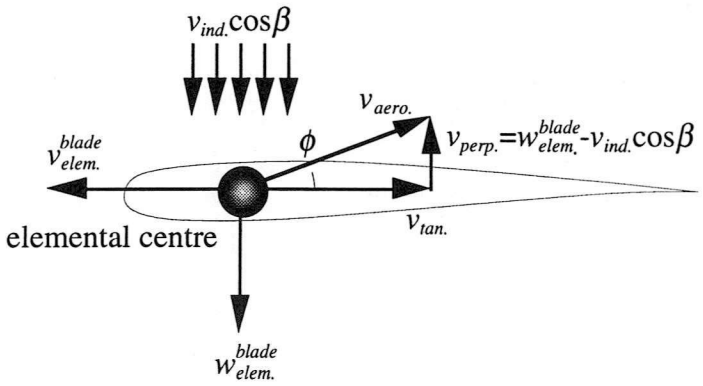

Figure 6 : Perpendicular Component of Velocity

The perpendicular component is not influenced by the direction of rotation and, as seen in Figure 6, can be expressed as follows :

$$v_{perp.} = w_{elem.}^{blade} - v_{ind.}\cos\beta,$$

where the induced velocity, $v_{ind.}$ is assumed to be composed of a uniform component over the whole disc, v_0 and harmonic components, v_{1s} and v_{1c} :

$$v_{ind.} = v_0 + \frac{r_{elem.}}{R}\left(v_{1s}\sin\psi + v_{1c}\cos\psi\right). \qquad (13)$$

The uniform induced velocity and the rotor thrust are interdependent and, as such, v_0 has to be solved iteratively. This process is described with the inflow model in Section 5.

Calculation of the elemental lift and drag requires knowledge of the local lift and drag coefficients. These can be found using look-up tables as functions of local Mach number, M and angle of attack, α. The local Mach number is determined by the ratio of the aerodynamic velocity - defined as the resultant of the tangential and perpendicular

velocity components - to the local speed of sound of air, a :

$$v_{aero.} = \sqrt{\left(v_{tan.}^2 + v_{perp.}^2\right)},$$

$$M = \frac{v_{aero.}}{a},$$

while the angle of attack (which through the inflow model implicitly considers induced effects) is the sum of the incidence of the elemental centre with respect to the airflow, ϕ, and the blade pitch angle, θ :

$$\alpha = \theta + \phi,$$

with the incidence defined as that relating the tangential and perpendicular velocities :

$$\phi = tan^{-1}\left(\frac{v_{perp.}}{v_{tan.}}\right).$$

Blade pitch angle, θ is composed of the pitch at the blade root - due to the collective, θ_0, longitudinal cyclic, θ_{1s} and lateral cyclic, θ_{1c} controls inputs - and the spanwise geometric twist, θ_{twist} :

$$\theta = \theta_{root} + \theta_{twist}\left(r_{elem.}\right),$$

where $$\theta_{root} = \theta_0 + \theta_{1s}\sin\psi + \theta_{1c}\cos\psi.$$

The geometic twist can be expressed as discrete values for each element or as a continuous (often linear) function. Thus linear interpolation of the aerodynamic look-up tables yields estimates of the lift and drag coefficients for each element and the associated forces per unit span can be calculated using expressions in the traditional aerodynamic form :

$$\bar{l}_{elem.} = \frac{1}{2}\rho v_{aero.}^2 c_{elem.} C_l(\alpha, M),$$
$$\bar{d}_{elem.} = \frac{1}{2}\rho v_{aero.}^2 c_{elem.} C_d(\alpha, M),$$

where ρ and $c_{elem.}$ are the air density and the blade element chord respectively.

The lift and drag - which are respectively perpendicular to and parallel with the

local velocity - are subseqently transformed using the angle of incidence, ϕ to find the aerodynamic forces per unit span referred to the blade axis set :

$$\underline{\bar{f}}_{aero.}^{blade} = \begin{Bmatrix} 0 \\ -n_{clock}\bar{d}_{elem.}\cos\phi + n_{clock}\bar{l}_{elem.}\sin\phi \\ -\bar{l}_{elem.}\cos\phi - \bar{d}_{elem.}\sin\phi \end{Bmatrix}.$$

In the limit (as unity $\rightarrow dr_{elem.} \rightarrow 0$) spanwise integration of these forces would allow evaluation of the aerodynamic forces acting over the entire blade, $\underline{F}_{aero.}^{blade}$. Due to the difficulty in expanding the above expressions algebraically with respect to $r_{elem.}$, however, the total blade forces are in practice estimated numerically. Numerical integration simply involves summing the aerodynamic forces acting on a finite number, $n_{elem.}$, of blade elements, length $\delta r_{elem.}$. Hence :

$$\underline{F}_{aero.}^{blade} = \int_{x_{hinge}}^{R} \underline{f}_{aero.}^{blade} dr_{elem.}$$

can be approximated by :

$$\underline{F}_{aero.}^{blade} = \sum_{k=1}^{n_{elem.}} \underline{f}_{aero._k}^{blade} \delta r_{elem._k} .$$

In order to find the total forces acting on each blade it is also necessary, of course, to include the inertial contribution to the forces which requires knowledge of the elemental accelerations derived in the previous section. Formulation of the inertial forces is embellished in the following section.

3.2.2 Inertial Force Acting Upon a Blade Element

Having calculated the acceleration of the centre point of the blade element then by Newton's 2nd Law the product of this and the elemental mass will yield the inertial force acting upon the element. Thus if $\overline{m}_{elem.}$ is the mass per unit span then the inertial force per unit span is given by the following expression :

$$\underline{\bar{f}}_{in.}^{blade} = \overline{m}_{elem.} \begin{Bmatrix} a_{x\,elem.}^{blade} \\ a_{y\,elem.}^{blade} \\ a_{z\,elem.}^{blade} \end{Bmatrix},$$

which, in common with the aerodynamic forces, is integrated numerically to estimate the inertial forces acting over the length of the blade :

$$\underline{F}_{in.}^{blade} = \sum_{k=1}^{n_{elem.}} \underline{f}_{in._k}^{blade} \delta r_{elem._k}.$$

The next stage is to calculate the forces and moments acting about the hub centre due to all of the blades.

3.2.3 Forces and Moments at Hub due to Blade Forces

What we first want to calculate is the force transmitted to the rotor by each blade via their respective hinges, $\underline{F}_{hinge}^{blade}$ i.e. the equal and opposite force to that supplied by the rotor. Thus applying Newton III to the m^{th} blade force equilibrium demands that the following is observed :

$$-\underline{F}_{hinge_m}^{blade} + \int_{x_{hinge}}^{R} \underline{f}_{aero.}^{blade} dr_{elem.} = \int_{x_{hinge}}^{R} \underline{f}_{in.}^{blade} dr_{elem.} \tag{14}$$

represented numerically by :

$$-\underline{F}_{hinge_m}^{blade} + \sum_{k=1}^{n_{elem.}} \underline{f}_{aero._k}^{blade} \delta r_{elem._k} = \sum_{k=1}^{n_{elem.}} \underline{f}_{in._k}^{blade} \delta r_{elem._k},$$

which when rearranged yields an expression for the forces from each of m blades acting upon the rotor :

$$\begin{aligned} \underline{F}_{hinge_m}^{blade} &= \sum_{k=1}^{n_{elem.}} \underline{f}_{aero._k}^{blade} \delta r_{elem._k} - \sum_{k=1}^{n_{elem.}} \underline{f}_{in._k}^{blade} \delta r_{elem._k} \\ &= \sum_{k=1}^{n_{elem.}} \underline{f}_{elem._k}^{blade} \delta r_{elem._k} \end{aligned}$$

The moment reactions are calculated by taking the cross product of the distance between each elemental force and the hinge :

$$\underline{M}_{hinge_m}^{blade} = \sum_{k=1}^{n_{elem.}} \left(\underline{r}_{hinge/elem._k}^{blade} \times \underline{f}_{elem._k}^{blade} \delta r_{elem._k} \right),$$

though in practice only the moment in the $x-y$ plane, $N_{hinge\, z_m}^{blade}$ need be considered due to the rotor assumptions stated earlier. To reiterate : the absence of lag freedom necessitates a restoring moment in the $x-y$ plane, the result of using an effective hinge offset however is that there is complete flap freedom (i.e. no restraining spring) and

consequently no moment in the $x-z$ plane for either a fully-articulated or semi-rigid rotor model. Additionally there is no torsional moment as the aerodynamic centre is assumed coincident with the centre line of the blade and the position vector, $\underline{r}^{blade}_{hinge/elem._k}$ has only an $\underline{i}^{blade}$ component. Having calculated the forces and moments produced by the blades they can now be resolved to establish the main rotor's contribution to the external forces and moments in the Euler equations of motion.

3.2.4 Main Rotor's Contribution to External Forces and Moment

The forces and moments acting on the main rotor's hinges can be manipulated to find their cumulative effect upon the rotor hub. Each blade's contribution is firstly transfomed, via the shaft axis set, to the non-rotating disc axis of which the hub is the centre - a process involving the transposes of the *shaft / blade* and *disc / shaft* transformation matrices from Section 3.1.1. As the hinge is not coincident with the hub the moments must be augmented with components due to the influence of the effective hinge offset. The constituents from each blade are then summed to find the total forces and moments, referred to disc axes, at the hub :

$$\underline{F}^{disc}_{hub} = \sum_{m=1}^{n_{blades}} \underline{F}^{disc}_{hinge_m}$$

$$= \sum_{m=1}^{n_{blades}} \left[T^{disc/shaft}\right]^{\mathrm{T}} \left[T^{shaft/blade}\right]^{\mathrm{T}} \underline{F}^{blade}_{hinge_m},$$

$$\underline{M}^{disc}_{hub} = \sum_{m=1}^{n_{blades}} \left(\left[T^{disc/shaft}\right]^{\mathrm{T}} \left[T^{shaft/blade}\right]^{\mathrm{T}} \underline{M}^{blade}_{hinge_m} + \underline{r}^{disc}_{hub/hinge_m} \times \underline{F}^{disc}_{hinge_m} \right).$$

These hub forces are then transformed from disc to body axes yielding the external forces acting at the helicopter centre of gravity due to the main rotor :

$$\underline{F}^{body}_{c.g.} = \left[T^{body/disc}\right]^{\mathrm{T}} \underline{F}^{disc}_{hub} = \begin{Bmatrix} X_{rotor} \\ Y_{rotor} \\ Z_{rotor} \end{Bmatrix}.$$

The moments are similarly transformed and the component due to the distance between the centre of gravity and the hub included. This supplies the main rotor's contribution to the external moments about the helicopter centre of gravity :

$$\underline{M}^{body}_{c.g.} = \left[T^{body/disc}\right]^{\mathrm{T}} \underline{M}^{disc}_{hub} + \underline{r}^{body}_{c.g./hub} \times \underline{F}^{body}_{c.g.} = \begin{Bmatrix} L_{rotor} \\ M_{rotor} \\ N_{rotor} \end{Bmatrix}.$$

4. Equations for Blade Flapping Dynamics

As with the forces in equation (14) the moments acting about each blade hinge must be in equilibrium. Assuming the hinge model desribed in Section 2 then there is no restoring moment (i.e. $\underline{M}_{hinge}^{blade} = \underline{0}$) and so the aerodynamic and inertial moments acting about the hinge must be equal :

$$\int_{x_{hinge}}^{R} \underline{r}_{hinge/elem.}^{blade} \times m_{elem.} \underline{a}_{elem.}^{blade} dr_{elem.} = \int_{x_{hinge}}^{R} \underline{r}_{hinge/elem.}^{blade} \times \underline{f}_{aero.}^{blade} dr_{elem.} . \qquad (15)$$

The right hand side of equation (15) is the forcing term and can be evaluated numerically in the same fashion as the moments transmitted to the main rotor :

$$\underline{M}_{hinge\ aero.}^{blade} = \sum_{k=1}^{n_{elem.}} \left(\underline{r}_{hinge/elem._k}^{blade} \times \underline{f}_{aero._k}^{blade} \delta r_{elem._k} \right) = \begin{Bmatrix} L_{aero.} \\ M_{aero.} \\ N_{aero.} \end{Bmatrix}.$$

The left hand side of equation (15) can be expanded to describe the flapping dynamics. Firstly consider the acceleration vector, $\underline{a}_{hinge}^{blade}$ which using small angle approximations - the cosine of an angle is equal to unity, the sine equal to the angle - can be expressed in terms of the shaft axes set including terms in β, $\dot{\beta}$ and $\ddot{\beta}$. Equation (16) :

$$\underline{a}_{elem.}^{blade} = \underline{a}_{hinge}^{blade} + \underline{\omega}^{blade} \times \left(\underline{\omega}^{blade} \times \underline{r}_{hinge/elem.}^{blade} \right) + \underline{\alpha}^{blade} \times \underline{r}_{hinge/elem.}^{blade}, \qquad (16)$$

and from equations (6), (10) and (12) :

$$\begin{aligned} \underline{a}_{elem.}^{blade} = & \left[T^{shaft/blade} \right] \underline{a}_{hinge}^{shaft} + \left(\left[T^{shaft/blade} \right] \underline{\omega}^{shaft} + \left\{ 0 \quad \dot{\beta} \quad 0 \right\}^{T} \right) \\ & \times \left(\left(\left[T^{shaft/blade} \right] \underline{\omega}^{shaft} + \left\{ 0 \quad \dot{\beta} \quad 0 \right\}^{T} \right) \times \underline{r}_{hinge/elem.}^{blade} \right) \\ & + \left(\left(\left[T^{shaft/blade} \right] \underline{\alpha}^{shaft} + \left\{ 0 \quad \ddot{\beta} \quad 0 \right\}^{T} \right) \times \underline{r}_{hinge/elem.}^{blade} \right), \end{aligned}$$

which upon further expansion, using equations (4) and (7), can be expressed as follows :

$$\underline{a}_{elem.}^{blade} = \begin{Bmatrix} a_{hinge\,x}^{shaft} - \beta a_{hinge\,z}^{shaft} \\ a_{hinge\,y}^{shaft} \\ \beta a_{hinge\,x}^{shaft} + a_{hinge\,z}^{shaft} \end{Bmatrix} + \begin{Bmatrix} -r_{elem.}\left(\left(q^{shaft} + \dot{\beta}\right)^2 + \left(\beta p^{shaft} + r^{shaft}\right)^2\right) \\ r_{elem.}\left(q^{shaft} + \dot{\beta}\right)\left(p^{shaft} - \beta r^{shaft}\right) \\ r_{elem.}\left(\beta p^{shaft} + r^{shaft}\right)\left(p^{shaft} - \beta r^{shaft}\right) \end{Bmatrix}$$
$$+ \begin{Bmatrix} 0 \\ r_{elem.}\left(\beta\alpha_x^{shaft} + \alpha_z^{shaft}\right) \\ -r_{elem.}\left(\alpha_y^{shaft} + \ddot{\beta}\right) \end{Bmatrix}. \qquad (17)$$

In the interests of clarity it is, perhaps, better to simplify the notation used in equation (17) yielding the following, more friendly expression :

$$\underline{a}_{element}^{blade} = \begin{Bmatrix} a_x - \beta a_z \\ a_y \\ \beta a_x + a_z \end{Bmatrix} + \begin{Bmatrix} -r_{elem.}\left(\left(q + \dot{\beta}\right)^2 + \left(\beta p + r\right)^2\right) \\ r_{elem.}\left(q + \dot{\beta}\right)\left(p - \beta r\right) \\ r_{elem.}\left(\beta p + r\right)\left(p - \beta r\right) \end{Bmatrix}$$
$$+ \begin{Bmatrix} 0 \\ r_{elem.}\left(\beta\alpha_x + \alpha_z\right) \\ -r_{elem.}\left(\alpha_y + \ddot{\beta}\right) \end{Bmatrix}. \qquad (18)$$

For blade flapping only the $\underline{j}^{blade}$ component resulting from the cross product on the left hand side of (15) need be considered. Thus substituting (18) and integrating equation (15) yields the following expression :

$$-M_\beta\left(\beta a_x + a_z\right) - I_\beta\left(\left(\beta p + r\right)\left(p - \beta r\right) - \left(\alpha_y + \ddot{\beta}\right)\right)\underline{j}^{blade} = M_{aero}\underline{j}^{blade} \qquad (19)$$

where $$M_\beta = \int_{x_{hinge}}^{R} m_{elem.} r_{elem.} dr_{elem.},$$

and $$I_\beta = \int_{x_{hinge}}^{R} m_{elem.} r_{elem.}^2 dr_{elem.}.$$

Finally equation (19) can be expanded and recast to produce the second order differential equation presented in (20) describing the dynamics of rotor blade flapping about a hinge. The term in K_β is included to take account of a hinge which is modelled with a restoring spring stiffness. Using the simpler notation :

$$\ddot{\beta} = -pr\beta^2 + \left(p^2 - r^2 + \frac{M_\beta}{I_\beta} a_x + \frac{K_\beta}{I_\beta} \right) \beta \qquad (20)$$
$$+ \left(pr - \alpha_y + \frac{M_\beta}{I_\beta} a_z \right) + \frac{M_{aero.}}{I_\beta},$$

and with the full notation :

$$\ddot{\beta} = -p^{shaft} r^{shaft} \beta^2 + \left(p^{shaft\,2} - r^{shaft\,2} + \frac{M_\beta}{I_\beta} a^{shaft}_{x\ hinge} + \frac{K_\beta}{I_\beta} \right) \beta$$
$$+ \left(p^{shaft} r^{shaft} - \alpha^{shaft}_y + \frac{M_\beta}{I_\beta} a^{shaft}_{z\ hinge} \right) + \frac{M_{aero.}}{I_\beta}.$$

5. The Peters - HaQuang Dynamic Inflow Model

The expression for the induced inflow velocity, $v_{ind.}$ referred to the rotor *disc* axis set is assumed to be of the form previously defined by equation (13) :

$$v_{ind.}(r_{elem.}, \psi) = v_0^{disc} + \frac{r_{elem.}}{R}\left(v_{1s}^{disc} \sin\psi + v_{1c}^{disc} \cos\psi\right),$$

where v_0^{disc}, v_{1s}^{disc} and v_{1c}^{disc} are the uniform, lateral and longitudinal variations respectively. This relationship, once the velocity components are known, is used in tandem with the motion of the blade relative to the disc plane to determine the instantaneous angle of attack, α of the centre of each blade element, see Section 3.2.1.

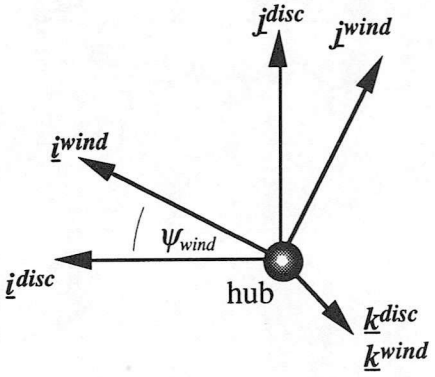

Figure 7 : Transformation from Disc to Wind Axis Set

For the purposes of the inflow calculations it is convenient to first consider all terms related to the *wind* axis set, i.e. velocities v_0^{wind}, $v_{1_s}^{wind}$ and $v_{1_c}^{wind}$, Figure 7. These values are non-dimensionalised using the rotor radius, R and the rotor speed, Ω ; the associated terms being λ_0^{wind}, $\lambda_{1_s}^{wind}$ and $\lambda_{1_c}^{wind}$. The velocity time histories are governed by the following first order differential equation :

$$[M]\begin{Bmatrix}\dot{\lambda}_0^{wind}\\ \dot{\lambda}_{1_s}^{wind}\\ \dot{\lambda}_{1_c}^{wind}\end{Bmatrix} + [L]_{nl}^{-1}\begin{Bmatrix}\lambda_0^{wind}\\ \lambda_{1_s}^{wind}\\ \lambda_{1_c}^{wind}\end{Bmatrix} = \begin{Bmatrix}C_T^{wind}\\ -C_L^{wind}\\ -C_M^{wind}\end{Bmatrix}_{aero.}, \qquad (21)$$

where $[M]$ is the apparent mass matrix and is defined as :

$$[M]=\begin{bmatrix} \frac{8}{3\pi} & 0 & 0 \\ 0 & -\frac{16}{45\pi} & 0 \\ 0 & 0 & -\frac{16}{45\pi} \end{bmatrix},$$

and $[L]_{nl}$ in the wind oriented, nonlinear, inflow gain matrix which relates the inflow components to the aerodynamic thrust, rolling and pitching moments coefficients. The matrix is non-diagonal representing the cross coupling that occurs between the inflow states. The inflow gains matrix is defined as :

$$[L]_{nl}=[L][\Lambda]^{-1},$$

where
$$[L]=\begin{bmatrix} \frac{1}{2} & 0 & \frac{15\pi}{64}\sqrt{\frac{1-\sin\chi}{1+\sin\chi}} \\ 0 & \frac{-4}{1+\sin\chi} & 0 \\ \frac{15\pi}{64}\sqrt{\frac{1-\sin\chi}{1+\sin\chi}} & 0 & \frac{-4\sin\chi}{1+\sin\chi} \end{bmatrix},$$

and
$$[\Lambda]=\begin{bmatrix} \lambda_{tot.} & 0 & 0 \\ 0 & \lambda_{cyc.} & 0 \\ 0 & 0 & \lambda_{cyc.} \end{bmatrix}.$$

The mass flow parameter matrix, $[\Lambda]$ contains the total resultant flow through the rotor disc, $\lambda_{tot.}$ and the mass flow parameter due to cyclic disturbances, $\lambda_{cyc.}$,

where
$$\lambda_{tot.}=\sqrt{\left(\mu^2+\left(\mu_z-\lambda_{mom.}\right)^2\right)},$$

and
$$\lambda_{cyc.}=\frac{\mu^2+\left(\mu_z-2\lambda_{mom.}\right)\left(\mu_z-\lambda_{mom.}\right)}{\lambda_{tot.}}.$$

The above unidentified terms are the non-dimensionalised momentum theory induced velocity due to the rotor thrust, $\lambda_{mom.}$ and the non-dimensionalised in-plane, μ and perpendicular, μ_z component disc velocities, Figure 8 :

$$\mu=\sqrt{\left(\mu_x^2+\mu_y^2\right)},$$

$$\mu_x = \frac{u_{hub}^{disc}}{\Omega R},$$

$$\mu_y = \frac{v_{hub}^{disc}}{\Omega R},$$

$$\mu_z = \frac{w_{hub}^{disc}}{\Omega R}.$$

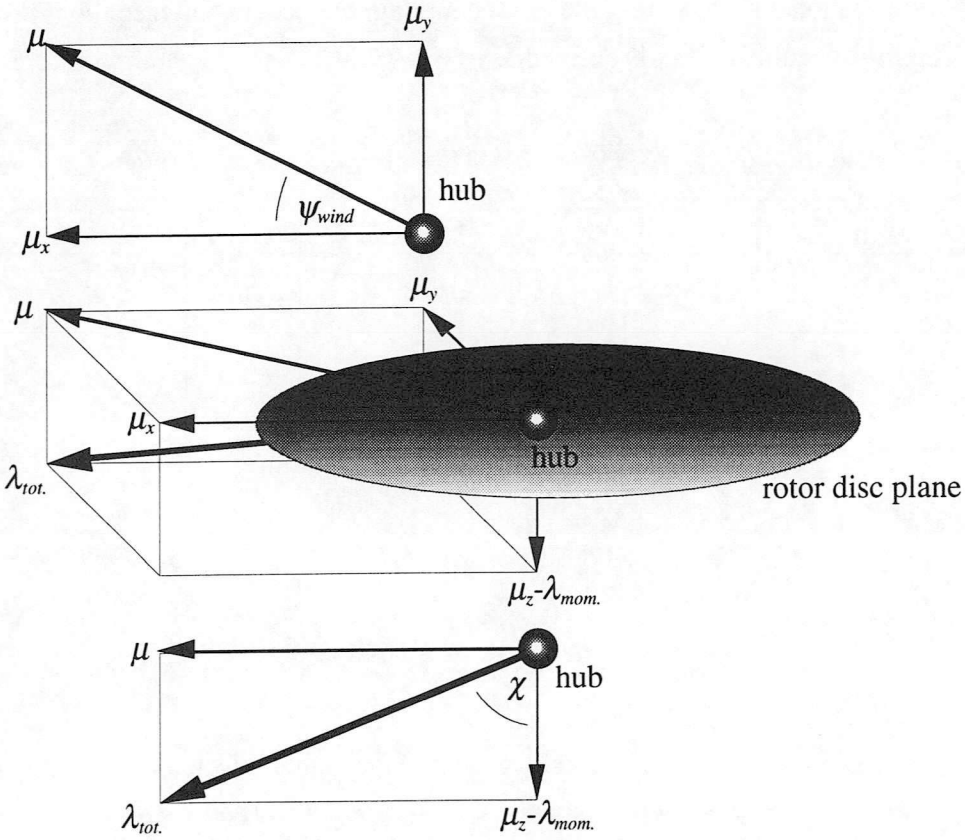

Figure 8 : Dimensionless Inflow Parameters; Wind Sideslip and Wake Angles

The wake angle, χ and the wind sideslip angle are defined respectively as :

$$\chi = \tan^{-1}\left(\frac{|\mu_z - \lambda_{mom.}|}{\mu}\right),$$

and

$$\psi_{wind} = \tan^{-1}\left\{\frac{\mu_y}{\mu_x}\right\}.$$

Using the subsequent relationships :

$$\begin{Bmatrix} C_T^{wind} \\ -C_L^{wind} \\ -C_M^{wind} \end{Bmatrix}_{aero.} = \left[T^{wind/disc}\right] \begin{Bmatrix} C_T^{disc} \\ -C_L^{disc} \\ -C_M^{disc} \end{Bmatrix}_{aero.},$$

$$\begin{Bmatrix} \lambda_0^{wind} \\ \lambda_{1_s}^{wind} \\ \lambda_{1_c}^{wind} \end{Bmatrix} = \left[T^{wind/disc}\right] \begin{Bmatrix} \lambda_0^{disc} \\ \lambda_{1_s}^{disc} \\ \lambda_{1_c}^{disc} \end{Bmatrix},$$

and

$$\left[T^{wind/disc}\right] = \begin{bmatrix} 1 & 0 & 0 \\ 0 & \cos\psi_{wind} & \sin\psi_{wind} \\ 0 & -\sin\psi_{wind} & \cos\psi_{wind} \end{bmatrix},$$

the theory can be transformed from the wind axes set to one aligned with the rotor disc. Upon expansion equation (21) becomes :

$$[M]\left[T^{wind/disc}\right] \begin{Bmatrix} \dot{\lambda}_0^{disc} \\ \dot{\lambda}_{1_s}^{disc} \\ \dot{\lambda}_{1_c}^{disc} \end{Bmatrix} + [\Lambda][L]^{-1}\left[T^{wind/disc}\right] \begin{Bmatrix} \lambda_0^{disc} \\ \lambda_{1_s}^{disc} \\ \lambda_{1_c}^{disc} \end{Bmatrix} = \left[T^{wind/disc}\right] \begin{Bmatrix} C_T^{disc} \\ -C_L^{disc} \\ -C_M^{disc} \end{Bmatrix}_{aero.} . \quad (22)$$

In order to remove the transformation matrix $\left[T^{wind/disc}\right]$ from the first term of Equation (22), the equation is multiplied by the transpose of the transformation matrix as follows :

$$\left[T^{wind/disc}\right]^{\mathrm{T}}[M]\left[T^{wind/disc}\right] \begin{Bmatrix} \dot{\lambda}_0^{disc} \\ \dot{\lambda}_{1_s}^{disc} \\ \dot{\lambda}_{1_c}^{disc} \end{Bmatrix} + \left[T^{wind/disc}\right]^{\mathrm{T}}[\Lambda][L]^{-1}\left[T^{wind/disc}\right] \begin{Bmatrix} \lambda_0^{disc} \\ \lambda_{1_s}^{disc} \\ \lambda_{1_c}^{disc} \end{Bmatrix} = \begin{Bmatrix} C_T^{disc} \\ -C_L^{disc} \\ -C_M^{disc} \end{Bmatrix}_{aero.} .$$

Because the first element of $\left[T^{wind/disc}\right]$ is unity, and both $[M]$ and $[\Lambda]$ are diagonal matrices, the order of multiplication can be reversed. The result of this is the first order differential equation representing the non-linear theory of dynamic inflow with respect to the rotor disc plane, equation (23) :

$$[M] \begin{Bmatrix} \dot{\lambda}_0^{disc} \\ \dot{\lambda}_{1_s}^{disc} \\ \dot{\lambda}_{1_c}^{disc} \end{Bmatrix} + \left[\hat{L}\right]^{-1} \begin{Bmatrix} \lambda_0^{disc} \\ \lambda_{1_s}^{disc} \\ \lambda_{1_c}^{disc} \end{Bmatrix} = \begin{Bmatrix} C_T^{disc} \\ -C_L^{disc} \\ -C_M^{disc} \end{Bmatrix}_{aero.} , \quad (23)$$

where $$\left[\hat{\boldsymbol{L}}\right]^{-1} = [\Lambda]\left[\boldsymbol{T}^{wind/disc}\right]^{\mathrm{T}}[\boldsymbol{L}]^{-1}\left[\boldsymbol{T}^{wind/disc}\right].$$

6. Conclusions

The individual blade model has been successfully implemented in inverse simulation. In addition the results have been verified against those of the existing HGS[1] disc model, and validated against flight data supplied by DRA, Bedford[8].

7. References

1. Thomson, D.G., "Development of a Generic Helicopter Mathematical Model for Application to Inverse Simulation", University of Glasgow, Department of Aerospace Engineering, Internal Report No. 9216, June 1992.

2. Houston, S., "Rotorcraft Aeromechanics Simulation for Control Analysis - Mathematical Model Definition", University of Glasgow, Department of Aerospace Engineering, Internal Report No. 9123, 1991.

3. Mansur, M.H., "Development and Validation of a Blade Element Mathamatical Model for the AH-64A Apache Helicopter", NASA-TM-108863, April 1995.

4. McCormick, B. W., "Aerodynamics Aeronautics and Flight Mechanics Second Edition", John Wiley and Sons, 1995.

5. Peters, D.A., HaQuang, N., "Dynamic Inflow for Practical Applications", Journal of the American Helicopter Society, Technical Note, pp. 64-68, October 1988.

6. Pitt, D.M., Peters, D.A., "Theoretical Prediction of Dynamic Inflow Derivatives", Vertica, Vol. 5, pp. 21-34, 1981.

7. Chen, R.T.N., "A Survey of Nonuniform Inflow Models for Rotorcraft Flight Dynamics and Control Applications", Paper 64, 15th European Rotorcraft Forum, Amsterdam, Netherlands, September 1989.

8. Rutherford, S., Thomson, D.G., "Helicopter Inverse Simulation Incorporating an Individual Blade Rotor Model", Paper 3.6.3, ICAS Congress, Sorrento, Italy, September 1996.

9. Turnour, S. R., Celi, R., "Modelling of Flexible Rotor Blades for Helicopter Flight Dynamics Applications", Journal of the American Helicopter Society, pp. 52-66, January 1996.

10. Lewis, W.D., "An Aeroelastic Model Structure Investigation for a Manned Real-Time Rotorcraft Simulation", American Helicopter Society 47th Annual Forum, St. Louis, MO, May 1993.

11. Sturisky, S.H., Schrange, D.P., "System Identification Validation of an AH-64 Aeroelastic Simulation Model", American Helicopter Society 47th Annual Forum, St. Louis, MO, May 1993.

12. Johnson, W., "Helicopter Theory", Dover Publishing, 1980.

13. Padfield, G.D., "A Theoretical Model of Helicopter Flight Mechanics for Application to Piloted Simulation", Royal Aircraft Establishment, TR 81048, April 1981.

14. Hill, G., Du Val, R.W., Green, J.A., Huynh, L.C., "A Piloted Comparison of Elastic and Rigid Blade-Element Rotor Models Using Parallel Processing Technology", Paper III.4.4.1, 16th European Rotorcraft Forum, Glasgow, U.K., September 1990.

Appendix 1 The Euler Rigid Body Equations of Motion

To simulate the motion of the helicopter's centre of gravity, the familiar Euler rigid body equations of motion are used :

$$\dot{U} = -(WQ - VR) + \frac{X}{m} - g\sin\theta,$$

$$\dot{V} = -(UR - WP) + \frac{Y}{m} + g\cos\theta\sin\phi,$$

$$\dot{W} = -(VP - UQ) + \frac{Z}{m} + g\cos\theta\cos\phi,$$

$$I_{xx}\dot{P} = (I_{yy} - I_{zz})QR + I_{xz}(\dot{R} + PQ) + L,$$

$$I_{yy}\dot{Q} = (I_{zz} - I_{xx})RP + I_{xz}(R^2 - P^2) + M,$$

$$I_{zz}\dot{R} = (I_{xx} - I_{yy})PQ + I_{xz}(\dot{P} - QR) + N.$$

where U, V, W are the components of translational velocity relative to the body fixed reference frame in the directions of the unit vectors $\underline{i}^{body}$, $\underline{j}^{body}$, $\underline{k}^{body}$ respectively ;

P, Q, R are rotational velocities about the body axes, positive directions consistent with a right handed axis set ;

ϕ, θ, ψ are the fuselage pitch, roll and yaw attitudes ;

m is the total mass of the helicopter ;

I_{xx}, I_{yy}, I_{zz} are the moments of inertia of the helicopter about the body axes ;

I_{xz} is the product of inertia of the helicopter ;

X, Y, Z are the external forces acting through the helicopter's centre of gravity in the $\underline{i}^{body}$, $\underline{j}^{body}$, $\underline{k}^{body}$ directions respectively;

and L, M, N are the external moments acting about the centre of gravity.

The rates of change of the attitude angles θ, ϕ, and ψ are related to the body axes rotational velocities P, Q and R by the kinematic expressions :

$$\dot{\phi} = P + Q\sin\phi\tan\theta + R\cos\phi\tan\theta,$$

$$\dot{\theta} = Q\cos\phi - R\sin\phi,$$

and $$\dot{\psi} = Q\sin\phi\sec\theta + R\cos\phi\sec\theta.$$

The earth fixed velocities $\dot{x}_e$, $\dot{y}_e$ and $\dot{z}_e$ can be calculated from the translational body fixed velocities U, V and W and the attitude angles θ, ϕ, and ψ by the Euler transformation equations :

$$\begin{bmatrix} \dot{x}_e \\ \dot{y}_e \\ \dot{z}_e \end{bmatrix} = \begin{bmatrix} l_1 & m_1 & n_1 \\ l_2 & m_2 & n_2 \\ l_3 & m_3 & n_3 \end{bmatrix} \begin{bmatrix} U \\ V \\ W \end{bmatrix},$$

where

$$l_1 = \cos\theta\cos\psi,$$
$$l_2 = \cos\theta\sin\psi,$$
$$l_3 = -\sin\theta,$$
$$m_1 = \sin\phi\sin\theta\cos\psi - \cos\phi\sin\psi,$$
$$m_2 = \sin\phi\sin\theta\sin\psi + \cos\phi\cos\psi,$$
$$m_3 = \sin\phi\cos\theta,$$
$$n_1 = \cos\phi\cos\theta\cos\psi + \sin\phi\sin\psi,$$
$$n_2 = \cos\phi\sin\theta\sin\psi - \sin\phi\cos\psi,$$

and $$n_3 = \cos\phi\cos\theta.$$